

## Article

# Post-Fire Restoration in Mediterranean Watersheds: Coupling WiMMed Modeling with LiDAR–Landsat Vegetation Recovery

Edward A. Velasco Pereira<sup>1</sup> and Rafael M<sup>a</sup> Navarro Cerrillo<sup>1,2,\*</sup> 

<sup>1</sup> Laboratory of Dendrochronology, Silviculture and Global Change, DendrodatLab-ERSAF, Department of Forest Engineering, Campus de Rabanales, University of Cordoba, Crta. IV, 14071 Córdoba, Spain

<sup>2</sup> Centro Nacional de Excelencia para la Industria de la Madera (CENAMAD)-ANID BASAL FB210015, Pontificia Universidad Católica de Chile, Av. Vicuña Mackenna 4860, Santiago 7820436, Chile

\* Correspondence: rmnnavarro@uco.es

## Highlights

### What are the main findings?

- Hydrological model–LiDAR integration captured post-fire hydrology changes.
- Runoff increased after wildfires but decreased as vegetation recovered.
- A Priority Post-Fire Restoration Index (PPRI) is proposed.

### What are the implications of the main findings?

- Remote sensing–hydrological model integration improved pre- and post-fire simulations.
- The PPRI helps to optimize post-fire restoration interventions.

## Abstract

Wildfires are among the most severe disturbances in Mediterranean ecosystems, altering vegetation structure, soil properties, and hydrological functioning. Understanding post-fire hydrological dynamics is crucial for predicting flood and erosion risks and vegetation restoration in fire-prone regions. This study investigates the hydrological responses of Mediterranean watersheds following a wildfire event by integrating WiMMed (Watershed Integrated Management in Mediterranean Environments), a distributed, physically based hydrological model, with high-resolution vegetation data derived from LiDAR and Landsat imagery. A Priority Post-Fire Restoration Index (PPRI) was calculated as the weighted sum of the six parameters runoff (mm), flow accumulation (mm), distance to drainage network (m), slope (%), erodibility (*K*), lithology, and LiDAR index under a sediment reduction and runoff peak reduction scenario. The post-fire hydrological processes modeled with WiMMed described the dynamics of surface runoff and soil moisture redistribution across the upper soil layers after fire, and their gradual attenuation with vegetation regrowth. The spatial distribution of the PPRI identified specific zones within the burned watershed that require urgent restoration measures (10% and 4.55% under sediment reduction and peak reduction scenarios, respectively). The combined use of process-based modeling and remote sensing offers valuable insights into watershed-scale hydrological resilience and supports the design of post-fire restoration strategies in Mediterranean landscapes.



Academic Editor: Ioannis Gitas

Received: 9 November 2025

Revised: 13 December 2025

Accepted: 18 December 2025

Published: 22 December 2025

**Copyright:** © 2025 by the authors.

Licensee MDPI, Basel, Switzerland.

This article is an open access article distributed under the terms and

conditions of the [Creative Commons](https://creativecommons.org/licenses/by/4.0/)

[Attribution \(CC BY\)](https://creativecommons.org/licenses/by/4.0/) license.

**Keywords:** wildfires; hydrological modeling; post-fire restoration; Landsat and ALS integration

## 1. Introduction

Forest fires are critical natural and artificial disturbances with a critical influence on terrestrial ecosystems and hydrological processes. Global warming and land-use changes are increasing fire frequency and severity; hence, understanding the hydrological consequences of wildfires has become a major concern in environmental science and watershed management [1,2]. Forest fires modify vegetation structure and soil and surface conditions, leading to chain effects on infiltration, runoff, erosion, and sediment transport dynamics at different spatial and temporal scales. In recent decades, Mediterranean regions have experienced a marked rise in both the frequency and intensity of wildfires, driven by warmer temperatures, prolonged droughts, and shifts in land-use patterns [3]. These trends are altering fire regimes in ways that exacerbate vegetation loss and soil degradation, amplifying short-term hydrological responses such as peak runoff, flash flooding, and sediment transport following fire events [2].

Wildfires disrupt hydrological processes, mainly due to the reduction in vegetation cover that protects and stabilizes soils and regulates evapotranspiration and interception at landscape scale. When vegetation cover is lost, soil becomes more exposed to the impact of rainfall, while reducing water uptake by plants, altering soil moisture regimes [4]. Fire heat can also cause soils to become temporarily water-repellent, reducing their ability to absorb rainfall and increasing surface runoff [5]. As a result, hydrological networks often have sharper peak flows, flash floods, and transport large amounts of sediments, moving them to downstream water bodies [6]. In the months that follow a fire, geomorphic activity typically intensifies—especially on steep slopes, where unstable, ash-covered soils and heavy rain can lead to landslides, debris flows, or gully erosion [7]. These post-fire processes reshape the terrain and often degrade water quality, with consequences for both aquatic habitats and human water resources.

Understanding how vegetation structure changes after a wildfire is crucial for properly parameterizing hydrological models and evaluating how the landscape recovers. Several studies have suggested that combining LiDAR (Light Detection and Ranging) data with Landsat satellite imagery provides an effective approach to detect and quantify these vegetation shifts [8]. LiDAR offers detailed three-dimensional information on canopy height, density, and vertical arrangement, which makes it especially useful for identifying subtle alterations in forest structure [8,9]. When these data are integrated with the multispectral information from Landsat—along with vegetation indices such as NDVI and NBR—it becomes possible to track both the structural and temporal dynamics of vegetation recovery [10]. This integrated remote-sensing approach enables precise mapping of burn severity, vegetation loss, and vegetation regrowth, all of which are essential for updating land-cover classifications in hydrological models. Moreover, LiDAR-derived indicators such as reductions in canopy height or surface roughness can be directly related to post-fire changes in rainfall interception, evapotranspiration, and surface flow resistance. Together, these datasets help create vegetation models that more accurately represent the vertical and spectral dimensions of fire-induced change, leading to improved simulations of post-fire hydrological behavior and erosion potential.

The long-term hydrological effects of forest fires depend on several interacting factors, including burn severity, rainfall patterns, vegetation recovery, and soil resilience. In many cases, these impacts can last for years, influencing baseflow, groundwater recharge, and catchment-scale hydrology well beyond the immediate post-fire period [11,12]. To better capture and quantify these complex processes, physically based and spatially distributed models, such as the Watershed Integrated Management for Mediterranean Environments (WiMMed), have become valuable analytical tools. WiMMed was specifically developed

to simulate water balance and surface processes in Mediterranean basins, accounting for spatial variations in soil properties, vegetation cover, topography, and climate [13].

This model is particularly useful for post-fire applications because it can incorporate fire-related changes in vegetation and soil characteristics, such as reduced canopy cover, increased surface roughness, and temporary water hydrophobicity, directly into its parameterization. WiMMed allows us to assess both short-term and persistent hydrological impacts of wildfire by representing processes like infiltration, evapotranspiration, overland flow, and sediment transport at fine spatial and temporal scales. Its modular design also facilitates the integration of remote sensing data and field observations, improving the calibration of post-fire simulations [13]. Since wildfires alter the landscape and disrupt hydrological connectivity, WiMMed can help identify critical source zones for erosion and runoff generation, guiding targeted management and risk reduction strategies in Mediterranean and other fire-prone regions [14]. Overall, wildfires substantially modify watershed behavior, often increasing runoff, peak flows, and sediment yields because of vegetation loss and soil degradation. Hydrological models such as WiMMed provide a robust framework for quantifying these effects and for testing the performance of restoration or mitigation measures under different climatic and geomorphic conditions [15]. These tools also support evidence-based decision-making and help design post-fire interventions oriented at minimizing erosion and promoting ecosystem recovery.

In this context, this study assessed how effectively the WiMMed model simulates post-wildfire hydrological processes at high spatial and temporal resolution, with the broader goal of improving our understanding of wildfire impacts on watershed management in Mediterranean environments. The specific objectives were as follows: (i) to analyze key hydrological processes, runoff, infiltration, evapotranspiration, and overland flow under post-fire conditions by applying the WiMMed model; (ii) to strengthen model calibration and validation by incorporating remote sensing data and field observations into the modular framework of WiMMed, thereby improving the accuracy of post-fire simulations; and (iii) to identify critical source areas for runoff and erosion within fire-affected catchments, providing insights to guide targeted restoration efforts in Mediterranean and other fire-prone landscapes. Given projections of increasing wildfire activity under changing climate conditions, integration of remote sensing on fire–hydrology interactions is becoming increasingly vital for post-fire restoration. A deeper understanding of these processes can enhance predictive modeling, inform post-fire restoration, and support adaptive management strategies that foster ecosystem resilience and safeguard water resources in vulnerable regions.

## 2. Materials and Methods

### 2.1. Study Area

The study area is located in the Sierra de Huétor (Granada, southern Spain, Figure 1, UTM ULX: 457343 to LRX: 473918 and ULY: 4129353 to LRY: 4118806, European Datum, zone 30N) and spans an elevation range between 1050 and 1900 m a.s.l., with most sub-basins situated between 1200 and 1600 m. The site is characterized by a transitional climate between Mediterranean semiarid and Mediterranean subhumid, with a mean annual precipitation of approximately 600 mm, and annual mean temperatures ranging between 7 and 17 °C. Lithology of the watershed is relatively homogeneous, with nearly 80% of the burned area underlain by carbonate formations (limestone, dolomites, and related carbonate stones). The remaining area is composed of acidic lithologies such as mica-schists, gneisses, phyllites, and slates. Soils are predominantly shallow, stony leptosols and regosols developed over Jurassic and Cretaceous limestones and marls, with locally deeper colluvial deposits in valley bottoms. The morphotopography is characterized by

steep hillslopes (20–45%), narrow ridgelines, and deeply incised drainage networks typical of karstic mountain ranges. These lithological and topographic features contribute to high hydrological connectivity and rapid runoff generation, conditions that amplify the effects of wildfire on post-fire hydrological dynamics. Vegetation cover before the wildfire was dominated by coniferous plantations of *Pinus pinaster* Ait. and *P. halepensis* Mill., established during the mid-20th century for soil protection. These stands coexisted with remnant patches of *Quercus ilex* L. woodlands, particularly on more stable slopes and in less disturbed areas, as well as extensive areas of Mediterranean shrublands composed of species such as *Rosmarinus officinalis* L., *Cistus* spp., and *Genista* spp.

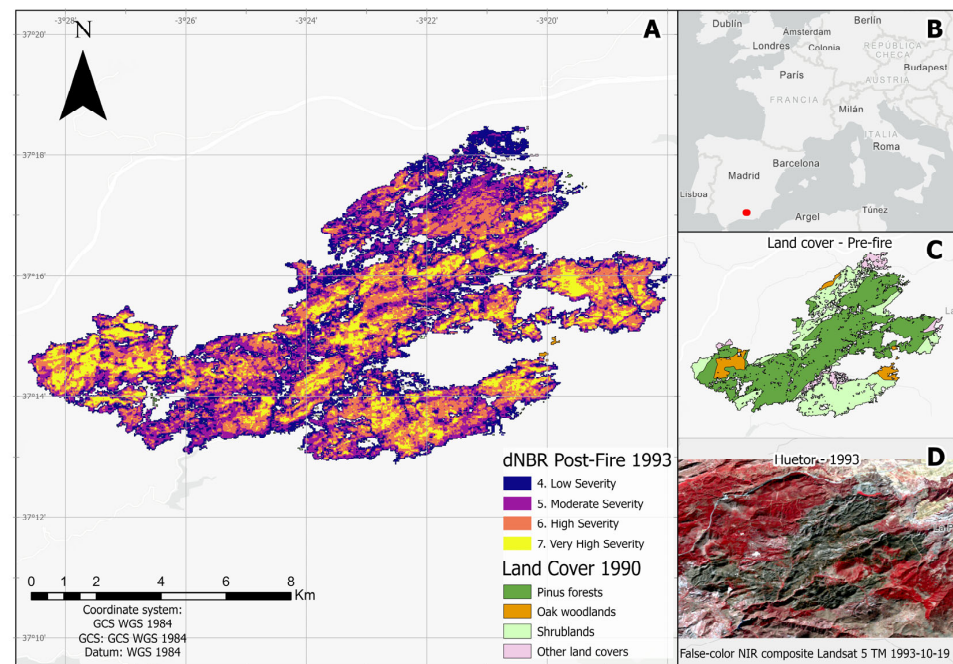


**Figure 1.** (A) Burn severity map and vegetation structure within the Sierra de Huétor study area. The background raster shows the differenced Normalized Burn Ratio (dNBR) classification of the 1993 wildfire, where severity classes correspond to the commonly used USGS Key & Benson scale [16] (0 = unburned, 1–3 = low, 4 = moderate, 5 = high, 6–7 = very high severity). (B) location of the study area (C) pre-fire vegetation cover (1990) Pine forests (*Pinus pinaster*, *P. halepensis*), Oak woodlands (*Quercus ilex*, *Q. faginea*), Shrublands (Mediterranean evergreen and semi-arid shrub species), and Other land cover (minor classes including riparian, herbaceous, or transitional vegetation) (D) fire perimeter. Unburned control areas used in the hydrological analyses correspond to watershed zones located outside the 1993 fire perimeter.

The study area was severely affected by a large wildfire in August 1993, which burned approximately 7000 ha. Fire severity was classified as extreme in 40%, moderate in 47%, and low in 13% of the affected surface area [17]. Post-fire restoration efforts were limited. An initial aerial sowing program carried out in 1996 produced poor results, while subsequent direct mechanical planting was sporadic and had little ecological impact. Therefore, much of the area has undergone natural regeneration, dominated by shrub encroachment, with partial recovery of *Pinus* stands and persistence of *Quercus ilex* patches.

## 2.2. Vegetation Data

This study used a pre-fire regional vegetation map based on photointerpretation of vegetation at 1:50,000 scale. Once forest types were assigned to a vegetation polygon, current vegetation cover, dominant and secondary tree species, and shrub species were added using the Information System on the Natural Heritage of Andalusia (SIPNA for its

Spanish initials, [18]). Forest boundary delimitation was reviewed using aerial photographs from the National Plan for Aerial Orthophotography of Spain (PNOA, National Geographic Institute of Spain, IGN) to detect changes in the forest areas. The process was conducted using ArcGIS Pro 3.0.

### 2.3. Remote Sensing Data Acquisition and Processing

The main methodological steps are illustrated in Figure 2. The methodology relies on two modeling components: (i) the LiDAR–Landsat regression models used to estimate annual vegetation structural variables (Mean Height, Vegetation Cover, LHDI) over the 1987–2020 period, and (ii) the WiMed distributed hydrological model, which incorporates these variables to simulate runoff, soil moisture, and subsurface flow dynamics. First, a set of forest structural variables were derived from ALS datasets: Mean Height (MH), Vegetation Cover (VC), and LiDAR height diversity index (LHDI) (Table S1 Supplementary Materials). Using these models, a 30-year Landsat-based time series was reconstructed to analyze the temporal dynamics of forest structural attributes according to [9]. The models were rigorously validated in both spatial and temporal dimensions using an independent dataset of ALS-derived variables (see [9]). The multitemporal ALS data were provided by the National Plan for Aerial Orthophotography of Spain [19]) with a nominal pulse density of  $\sim 0.5$  returns  $m^{-2}$  ETRS89 and UTM coordinate system (Table S2 Supplementary Materials). ALS data were processed using LAsTools version v180520 [20] and lidR R package [21].

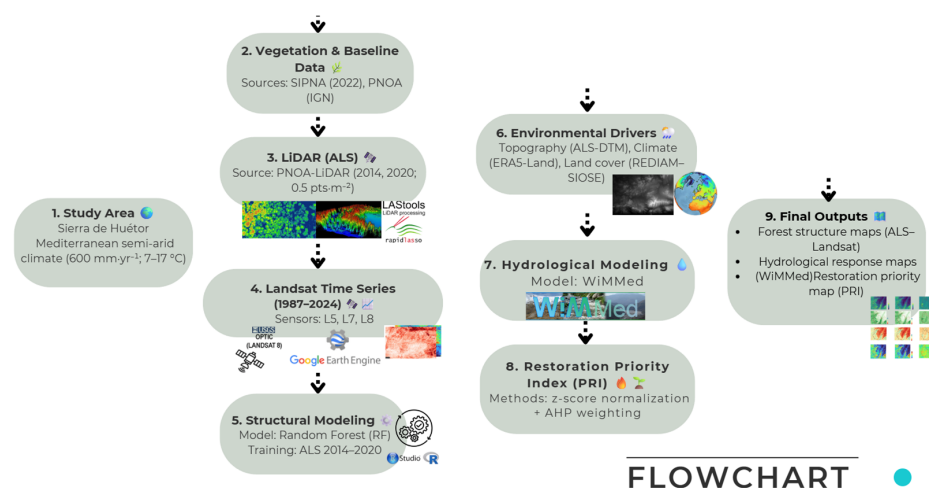


**Figure 2.** Flowchart used to develop Priority Post-fire Restoration Index in Mediterranean watersheds.

Satellite imagery from Landsat was selected (Landsat 5 TM for the 1987–2011 period; Landsat 7 ETM + for the 2012–2016 period and Landsat 8 OLI/TIRS for the 2013–2024 period) from the Google Earth Engine platform (GEE, <https://earthengine.google.com/>, accessed on 1 September 2024). The Earth Engine Python API version 1.1.2, integrated with the Python programming language, was used to streamline interactions with the Earth Engine servers and automate analytical workflows. Inter-sensor harmonization was performed to account for differences between Landsat satellite and normalized spectral characteristics using a multilinear regression approach [22]. To mitigate the effects of terrain slope, the topographic correction method SCS+C was applied, which is specifically designed for forested landscapes [23]. All Landsat imagery was corrected for topographic illumination effects using the SCS+C method of Soenen et al. [23]. Illumination geometry (solar zenith/azimuth and local incidence angle) was derived from a 5 m DEM. The C-parameter was obtained empirically for each Landsat sensor (TM, ETM+, OLI) by regressing reflectance against the cosine of the incidence angle using invariant targets located

on north-facing slopes. Because C-values are determined by sensor characteristics and terrain geometry, rather than vegetation condition, the same C-values were applied to pre- and post-fire images for each sensor. To ensure temporal consistency across the 1987–2020 Landsat series, inter-sensor harmonization was performed using multilinear regression between overlapping scenes from consecutive sensors, following common cross-calibration procedures used for long-term Landsat time series.

All geospatial datasets were harmonized to a common spatial resolution of 30 m prior to analysis. LiDAR-derived structural metrics, originally computed at 1 m, were aggregated to 30 m using mean and canopy-cover operators to match the Landsat grid. Soil maps and lithological layers were rasterized at 30 m using nearest-neighbor assignment to preserve categorical integrity. This harmonization ensured that the vegetation structural trajectories and static environmental layers were compatible with the spatial scale of the hydrological model inputs.

#### *2.4. Trends in Canopy Height and Cover Recovery After Fire*

To assess temporal trends in forest and vegetation structural parameters following the 1993 fire event across vegetation types, ALS-derived models were inverted and generalized to be compatible with a Landsat-based time series [9]. The incorporation of the detailed temporal changes of structural forest variables provided by ALS into the Landsat temporal framework allowed us to analyze post-fire vegetation dynamics over extended periods (20–30 years) and across diverse vegetation types (pine, oak and shrublands, Table S2 Supplementary Materials).

Data characterizing a range of environmental and forest attribute variables were collected (Table S3 Supplementary Materials) from a 30 × 30 m grid covering the study area. This resolution was considered sufficient to capture the spatial variability of post-fire regeneration drivers. Topographic variables (elevation, slope, aspect and topographic wetness index, TWI [24]) were obtained from a digital terrain model (DTM) generated from ALS data (2018) using the library raster in R version 4.5.2 [20,21]. Those variables are commonly used in post-fire recovery models [25] as proxies for key environmental constraints on species regeneration and growth. In addition, spatially explicit climatic variables were downloaded from the Environmental Information Network of Andalusia (REDIAM, ref. [26]).

#### *2.5. Hydrological Model*

Post-fire hydrological trends were assessed using the WiMMed model [13]. WiMMed is specifically designed for Mediterranean water catchments, since it incorporates spatial variability in climate, soil, topography, and vegetation. The model simulates the main components of the hydrological cycle (interception, evapotranspiration, infiltration, runoff, and baseflow) at the sub-basin scale, with temporal resolution suitable for long-term trend analysis. A schematic flowchart of the WiMMed model structure can be consulted in the Supplementary Materials (Figure S1). The WiMMed model has been previously calibrated and validated in multiple Andalusian Mediterranean catchments demonstrating its suitability for hydrological applications under the regional environmental conditions of southern Spain [13,14,27].

The model was implemented using spatially explicit inputs including the following: (i) Digital Elevation Model (DEM) for watershed delineation and slope, soil map and hydraulic properties; (ii) vegetation cover maps, derived from ALS-Landsat models after fire disturbance; and (iii) meteorological data (precipitation, temperature, solar radiation, humidity, and wind speed). Climatic data were obtained from the ERA5-Land dataset (ECMWF/ERA5\_LAND/DAILY\_AGGR collection) available in Google Earth Engine, at a

regular spatial resolution of 9 km for Andalusia (Table S3 Supplementary Materials). This collection provides daily time series from 1950 to approximately three months before the present, comprising more than fifty reanalysis-derived climatic variables. The variables retrieved included total precipitation, air temperature (mean, minimum, and maximum) at 2 m, dew point temperature, surface pressure, solar radiation, and wind components ( $u$  and  $v$ ) at 10 m height. Data were extracted for control points distributed across the watershed using spatial reduction over each point. The use of ERA5-Land ensured temporally continuous and spatially homogeneous climatic records, overcoming the limitations of conventional meteorological stations (incomplete series, temporal gaps, or limited spatial coverage during the study period). To harmonize the data for hydrological modeling, climatic variables were downscaled to the 30 m modeling grid using inverse-distance weighting (IDW) applied to a dense set of control points and corrected for elevation-driven temperature and precipitation gradients. Then, precipitation and temperature were topographically adjusted using lapse rates derived from long-term regional records, improving the representation of local climatic variability. Daily temporal aggregation further reduced the influence of sub-pixel variability. The downscaled fields were then used as distributed inputs for the runoff, interception, and evapotranspiration modules. The resulting interpolated fields were then used as distributed meteorological inputs for WiMMed. Potential uncertainties associated with the low spatial resolution of ERA5-Land were mitigated by using temporally aggregated daily data, less sensitive to sub-grid variability, and by calibrating the most climate-sensitive parameters ( $K_s$ ,  $S_{max}$ ,  $ET/ET_0$ ) so that simulated pre-fire hydrological behavior matched observed temporal patterns. This approach ensures that climatic forcing adequately captures watershed-scale variability required for long-term hydrological simulations. Subsequently, the extracted variables were processed in R [28] to derive the meteorological inputs required by the WiMMed model.

To incorporate the effects of fire severity on hydrological functioning, soil and surface parameters were initialized using the burn severity map (Figure 1A). In middle and high-severity areas, saturated hydraulic conductivity ( $K_s$ ) was reduced by 30–50% relative to pre-fire values, surface roughness (Manning's  $n$ ) was decreased to represent litter loss, and a temporary hydrophobicity factor was applied to limit infiltration during the first 1–2 years after the fire, following parameter ranges documented for Mediterranean soils (ref. [29], Table S4 Supplementary Materials). Moderate-severity areas received intermediate adjustments, while low-severity areas retained pre-fire soil values. These severity-dependent parameter changes ensured that the model represented both vegetation removal and soil structural degradation immediately after the fire.

Post-fire changes in vegetation cover were represented through the temporal trends in vegetation structural parameters (see Section 2.4) [9]. Calibration of the WiMMed hydrological model focused on the main parameters influencing runoff generation. Saturated hydraulic conductivity ( $K_s$ ) was adjusted to represent soil infiltration capacity, while the maximum canopy storage ( $S_{max}$ ) was optimized to account for rainfall interception and surface water retention. Surface roughness was defined using spatially distributed Manning coefficients derived from land cover data. In addition, the evapotranspiration coefficient ( $ET$ ) was calibrated relative to the reference evapotranspiration ( $ET_0$ ) to better represent vegetation water use under post-fire conditions. The rationale behind key parameter values was guided by previous applications of WiMMed in Mediterranean environments and by field-based soil and vegetation characteristics of the study area [13]. The LiDAR–Landsat reconstruction provided annual estimates of canopy height, vegetation cover, and structural diversity (LHDI), allowing vegetation-driven parameters in WiMMed to evolve dynamically over the simulation period. Specifically, maximum canopy storage ( $S_{max}$ ), interception capacity, and evapotranspiration (through  $ET/ET_0$ ) were updated each

year based on the reconstructed vegetation structure. Surface roughness (Manning's  $n$ ) was similarly adjusted to reflect temporal changes in shrub encroachment, pine regeneration, and oak persistence. This approach ensured that vegetation evolution, both abrupt post-fire loss and progressive recovery, was explicitly translated into hydrological parameterization. These externally validated datasets reduced parameter uncertainty and improved model realism.

The calibrated model was then applied to simulate hydrological processes over selected years representing (i) the last full pre-fire year (1992), (ii) the first post-fire year (1993), and (iii) key stages of vegetation and hydrological recovery: early post-fire (1998), mid-recovery (2008), and long-term recovery (2018). These time points capture the non-linear dynamics of post-fire ecosystem stabilization documented for Mediterranean landscapes between burned and unburned areas. Unburned reference areas correspond to the portions of the watershed outside the 1993 fire perimeter (see Figure 1A), primarily located on similar elevation, soil types, and vegetation composition. These zones experienced no fire disturbance and therefore provided a robust baseline for hydrological comparisons. Key simulated variables included: Exp, accumulated direct runoff (mm); HSol1, instantaneous annual mean soil moisture in the surface layer (0–25 cm, mm); HSol2, instantaneous soil moisture in the deeper layer (mm); Inf, accumulated infiltration from the surface into the soil (mm); and Qlat, accumulated lateral flow, representing the horizontal movement of water between cells (mm) (Table S5, Supplementary Materials). A preliminary parameter sensitivity analysis was conducted by varying  $K_s$ ,  $S_{max}$ , Manning's  $n$ , and  $ET/ET_0 \pm 20\%$  around their calibrated values. Results showed that  $K_s$  and  $S_{max}$  exerted the greatest influence on simulated direct runoff (Exp) and surface soil moisture (HSol1), while Manning's  $n$  primarily affected accumulated lateral flow (Qlat). The  $ET/ET_0$  coefficient moderately influenced evapotranspiration rates but had limited impact on runoff at the event scale. These sensitivity patterns were consistent with the hydrological behavior of semi-arid Mediterranean basins and confirm the appropriateness of focusing calibration efforts on infiltration and interception-related parameters.

Although vegetation recovery constitutes a major control on post-fire hydrological processes, the model also incorporates additional fire-induced alterations that influence runoff and soil moisture. Burn severity (Figure 1A) was used to adjust initial soil hydraulic properties, including temporary reductions in saturated hydraulic conductivity and increased hydrophobicity in high-severity areas, following parameter ranges reported for Mediterranean soils under severe wildfire conditions. Similarly, early post-fire reductions in surface roughness were represented through modified Manning coefficients. Meteorological variability between periods was accounted for by using full multi-decadal climate forcing (1987–2020), ensuring that pre–post differences reflect both vegetation change and interannual climate variability.

Temporal changes in hydrological behavior were evaluated using two complementary analytical approaches. First, a bitemporal analysis within the burned area was conducted by comparing pre-fire simulations (1987–1992) with post-fire simulations (1994–2020) to assess long-term changes associated with wildfire disturbance and vegetation recovery. Second, a spatial comparison between burned and unburned (control) areas was performed for selected representative years (1992, 1993, 1998, 2008, and 2018) for each hydrological variable (Exp, HSol1, HSol2, Qlat) to detect deviations associated with vegetation loss and subsequent regrowth. Unburned control areas were defined as grid cells ( $30 \times 30$  m) located outside the 1993 fire perimeter (Figure 1A). These areas were selected through a multi-criteria comparison with the unburned area including similar elevation ranges, soil types, lithology, slope gradients, and pre-fire vegetation composition. By constraining reference areas within the same watershed and matching key physiographic and ecological

attributes, we ensured that unburned areas provided an appropriate baseline for assessing post-fire hydrological deviations attributable to wildfire disturbance rather than to inherent landscape differences. In total, the control dataset comprised 1222 grid cells, while the burned area comprised 424 grid cells, providing a statistically robust basis for comparison.

The Mann–Whitney U test was applied in both analytical contexts. Within the burned area, it was used to test for statistically significant differences between pre- and post-fire distributions of simulated hydrological variables (Exp, HSol1, HSol2, and Qlat). In addition, for each representative year, the test was used to compare burned and unburned areas to evaluate post-fire deviations from baseline hydrological behavior. To satisfy the assumptions of the Mann–Whitney U test, statistical analyses were conducted considering spatially independent grid-cell values for each hydrological variable. Annual hydrological outputs were first aggregated at the grid-cell level, and comparisons were performed using multi-year period summaries, avoiding repeated-measures testing on the same spatial unit. This approach minimizes spatial and temporal autocorrelation effects and ensures that observations within each group can be reasonably treated as independent. The non-parametric Mann–Whitney U test was therefore appropriate for assessing differences between burned and unburned areas and between pre- and post-fire periods ( $p < 0.05$ ).

### 2.6. Long-Term Post-Fire Restoration Priorities

The objective of assigning areas of restoration priority was to reduce runoff peaks and/or volumes of sediment transport—by concentrating restoration actions in critical areas. The following layers were considered: runoff (mm), flow accumulation (mm), distance to drainage network (m), slope (%), erodibility ( $K$ ), lithology, and LiDAR index. The LiDAR index was derived from a weighted combination of structural metrics—Mean Height (0.7), Tree Cover (0.2), and LiDAR Height Diversity Index (LHDI, 0.1)—representing vegetation height, canopy density, and vertical complexity, respectively). All layers were normalized and standardized (z-score). A Priority Post-Fire Restoration Index (PPRI) was calculated as the weighted sum of the six partial indices (Equation (1)):

$$\text{Priority Post-fire Restoration Index} = \alpha \times \text{Runoff} + \beta \times \text{flow accumulation} + \mu \times \text{distance to drainage network} + \gamma \times \text{slope} + \delta \times \text{erodibility factor } k + \varepsilon \times \text{lithology} + \eta \times \text{Lidar} \quad (1)$$

where  $\alpha$ ,  $\beta$ ,  $\mu$ ,  $\gamma$ ,  $\delta$ ,  $\varepsilon$ , and  $\eta$  are the weighting factors. Statistical weights based on expert weights and analytic hierarchy process (AHP) were applied to determine the global ranking score of each indicator of the risk components [30]. Twenty-one forest and restoration technical managers of the Andalusian Forest Department were consulted. The areas of expertise of these technicians were fundamentally forestry, restoration and conservation technicians. Two restoration priorities scenarios were established: first, a reduction in runoff peaks, and second, a reduction in sedimentation. Consistency in decision-making was verified and bias in the process was reduced by calculating a consistency ratio (CR) using Equations (2) and (3).

$$CR = \frac{CI}{RI} \quad (2)$$

$$CI = \frac{\lambda_{\max} - n}{n - 1} \quad (3)$$

where CI is the consistency index and RI is the random index in Equation (2).  $\lambda_{\max}$  is the maximum average value obtained after dividing the sum of the weights, and  $n$  is the number of criteria. CR values of 0.10 and lower are considered tolerable [30]. To improve transparency of the weighting process, the aggregated pairwise comparison matrices generated from expert input are provided in the Supplementary Materials (Tables S6 and S7).

These matrices represent the mean pairwise scores across twenty-one forest and restoration specialists and form the basis for calculating the final AHP weights.

The PPRI was mapped on a continuous-category scale, generating a priority restoration map. The resulting map was simplified by assigning a threshold value of the PPRI to obtain thematic maps with the priority post-fire restoration areas. To avoid “riparian bias” and distribute PPRI by sub-basin, the 20% top pixels within each sub-basin were selected to ensure spatial balance and require minimum contiguity (e.g., 0.5–1 ha patches). Selecting the top 20% of PPRI values within each sub-basin was based on its frequent use in spatial prioritization studies to delineate high-risk areas without generating excessive fragmentation [31]. This approach avoids bias toward larger sub-basins and facilitates practical field implementation of restoration measures.

### 3. Results

#### 3.1. Post-Fire Hydrological Processes

The simulation of post-fire hydrological processes with WiMMed revealed clear dynamics in surface runoff and soil moisture redistribution across the upper soil layers (Figure 3). Figure 3A depicts the relationship between annual precipitation and instantaneous soil moisture in surface layer 1 (HSol1, mm) for burned and unburned areas across five representative years (1992, 1993, 1998, 2008, and 2018). Statistical comparisons confirmed that burned areas exhibited significantly higher soil moisture in the surface layer (HSol1) than unburned areas during the early post-fire years (1993–1998; Mann–Whitney U,  $p < 0.01$ ), consistent with reduced transpiration and altered infiltration conditions immediately after the disturbance. In 2008, differences between burned and unburned areas were considerably smaller ( $p > 0.05$ ), and by 2018, soil moisture–precipitation relationships were nearly indistinguishable between burned and unburned areas ( $p > 0.05$ ). This response indicated the reestablishment of pre-fire hydrological functioning, driven by vegetation regrowth and restoration of soil structure and permeability. In contrast, instantaneous soil moisture in deep layer 2 (HSol2) showed more attenuated variations, suggesting a buffering effect of deeper horizons and a delayed in hydrological response (Figure 3B). By 2008, differences in both soil layers between burned and unburned areas were no longer statistically significant ( $p > 0.05$ ), indicating a return toward pre-fire hydrological conditions as vegetation recovered. This vertical differentiation in soil moisture dynamics indicates that post-fire infiltration processes were restricted to shallow soil layers, limiting percolation into deeper soil compartments.

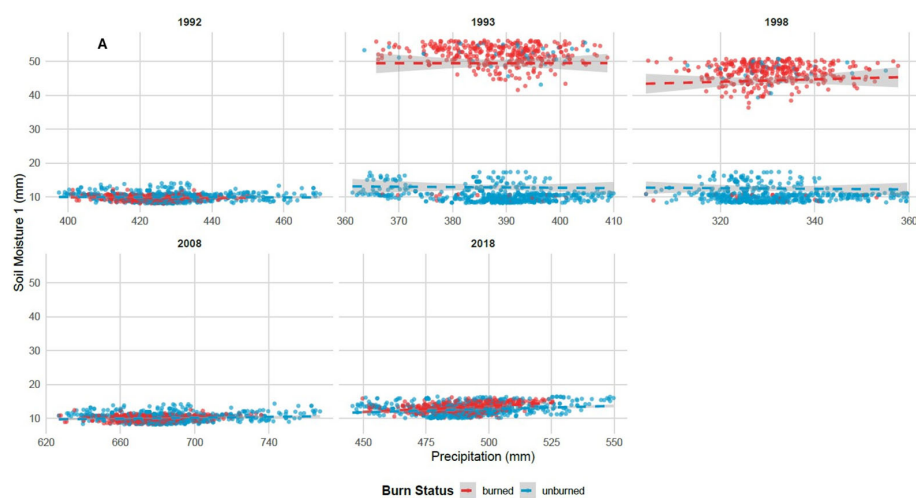
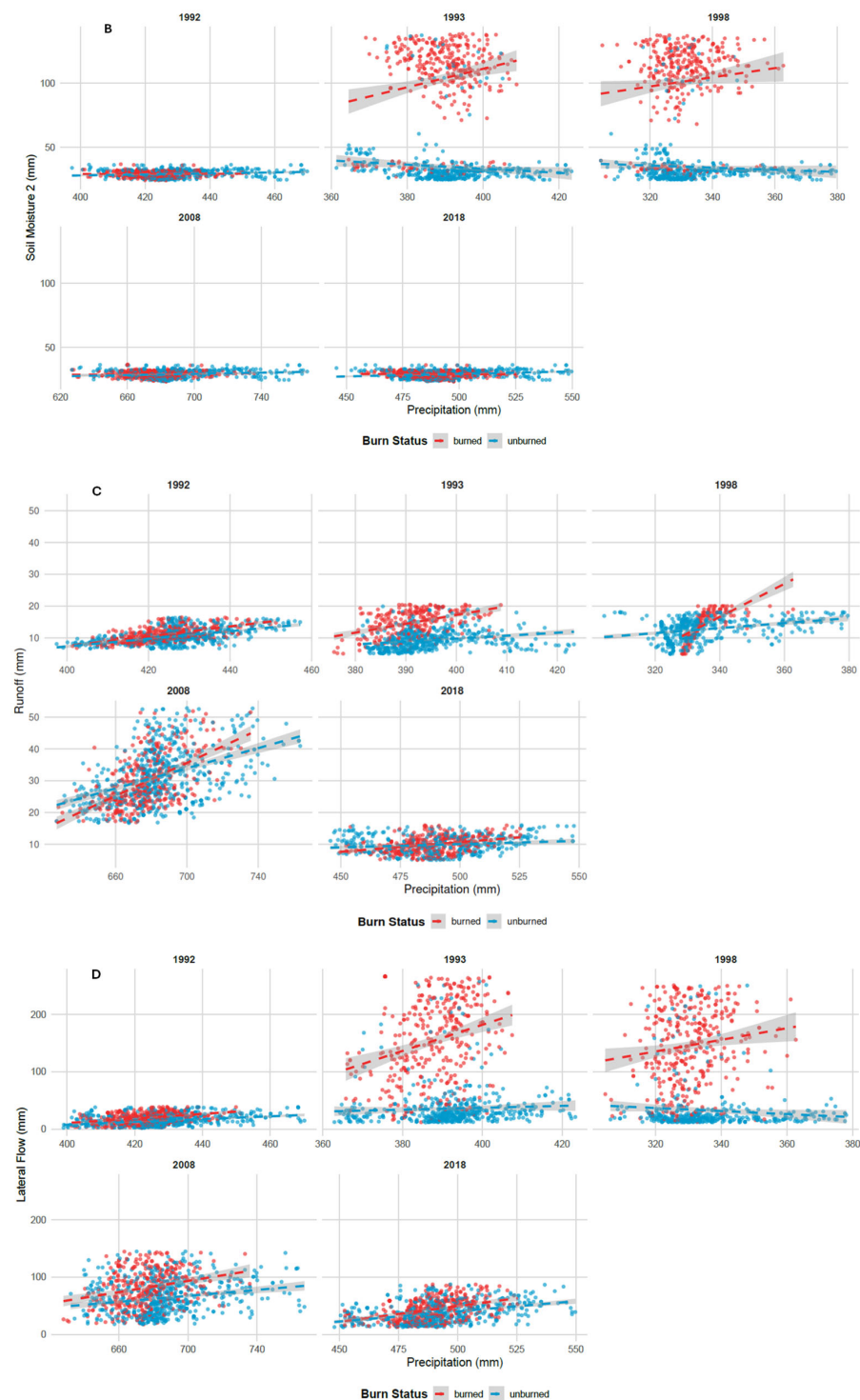


Figure 3. Cont.



**Figure 3.** Relationship between annual precipitation and post-fire hydrological variables simulated using WiMMed (Watershed Integrated Management for Mediterranean Environments). before and after the 1993 wildfire. Subplot labels (A–D) correspond to the following: (A) Instantaneous soil moisture in surface layer 1 (upper 25 cm, mm, Soil moisture1) (B) and deep layer (mm, Soil moisture2), (C) accumulated direct runoff (Exp, mm), and (D) accumulated lateral flow (Q<sub>lat</sub>, mm) for burned and unburned areas across five representative years (1992, 1993, 1998, 2008, and 2018) in Sierra de Hueter, Spain). Each panel shows the annual values of the corresponding variable along with trend and variability summaries. Dashed lines represent the fitted temporal trend (Sen’s slope-based regression) for the post-fire period, or the pre-fire baseline depending on the panel. Shaded envelopes represent the interannual variability expressed as  $\pm 1$  standard deviation (or 95% confidence interval) around the mean annual value.

Runoff (Exp) also showed statistically non significant increases in burned areas relative to unburned areas immediately following the fire (1993–1998;  $p > 0.05$ ) matching the trend toward hydrological recovery (Figure 3C). In 1992, prior to fire disturbance, runoff values were low and similar between burn and unburned areas, indicating comparable hydrological conditions. Following wildfire events, a sharp increase in runoff was observed in burned areas, particularly in 1993, when burned sites generated higher runoff for equivalent precipitation than the unburned areas. In 2008, runoff values in both burned and unburned areas became more comparable, suggesting ongoing hydrological stabilization. By 2018, differences between burn and unburned areas were minimal, with both areas having similar runoff–precipitation relationships. The analysis of soil moisture further supported this interpretation. Soil moisture in surface layer (HSol1), representing the shallowest horizon, displayed pronounced fluctuations in parallel to rainfall and runoff events, which was consistent with its exposure to altered surface conditions after fire. By contrast, HSol2 exhibited attenuated responses, showing slower and smaller changes in volumetric water content. This vertical gradient suggests that infiltration was largely restricted to upper soil horizons, limiting recharge of deeper layers under post-fire conditions.

Lateral flow (Qlat) also displayed significant differences in the early post-fire period ( $p < 0.05$ ), but convergence between burned and unburned areas by the late 2000s was supported by the absence of significant differences ( $p > 0.05$ ) (Figure 3D). In 1992, prior to the fire disturbance, the area showed similarly low Qlat values, indicating comparable hydrological behavior under intact vegetation and soil conditions. By 1998, burned areas still exhibited higher Qlat than unburned areas, though with reduced variance, suggesting the onset of hydrological recovery associated with partial vegetation regrowth and soil stabilization. The convergence observed in 2008, and particularly in 2018, indicates a gradual return toward pre-fire hydrological functioning. In the latter years, Qlat responses to precipitation were similar in burned and unburned areas, meaning reestablishment of vegetation cover and recovery of infiltration and water retention capacities.

### 3.2. Post-Fire Runoff Map

Spatial distribution of accumulated runoff between 1987 and 1993 ranged from 63.4 to 302.5 mm (Figure 4a). Areas with *Pinus* forests generally corresponded to intermediate to lower runoff values, reflecting higher canopy interception and infiltration capacity. In contrast, shrub-dominated areas exhibited comparatively higher runoff, which is consistent with their reduced structural cover and lower soil water retention. Oak forests showed an intermediate behavior, with runoff values in line with their mixed canopy and understory structure.

Twenty-five years after the wildfire (Figure 4b), modeled runoff (2014–2020) with WiMMed showed substantial changes in watershed and hydrological response. Land cover composition shifted markedly compared to pre-fire conditions. Areas previously dominated by *Pinus* showed a mosaic of vegetation recovery, with large expansion of shrublands and localized persistence of oak forests, while *Pinus* forests remained fragmented. These vegetation changes were translated into runoff dynamics. The accumulated runoff in 2014–2020 ranged from 67.4 to 295.8 mm, with higher values associated with shrub-dominated zones and lower values in areas of post-fire established tree forest cover. Compared with the pre-fire baseline (1987–1993), the overall pattern indicates a reduction in canopy-mediated regulation of runoff and an increase in spatial heterogeneity.

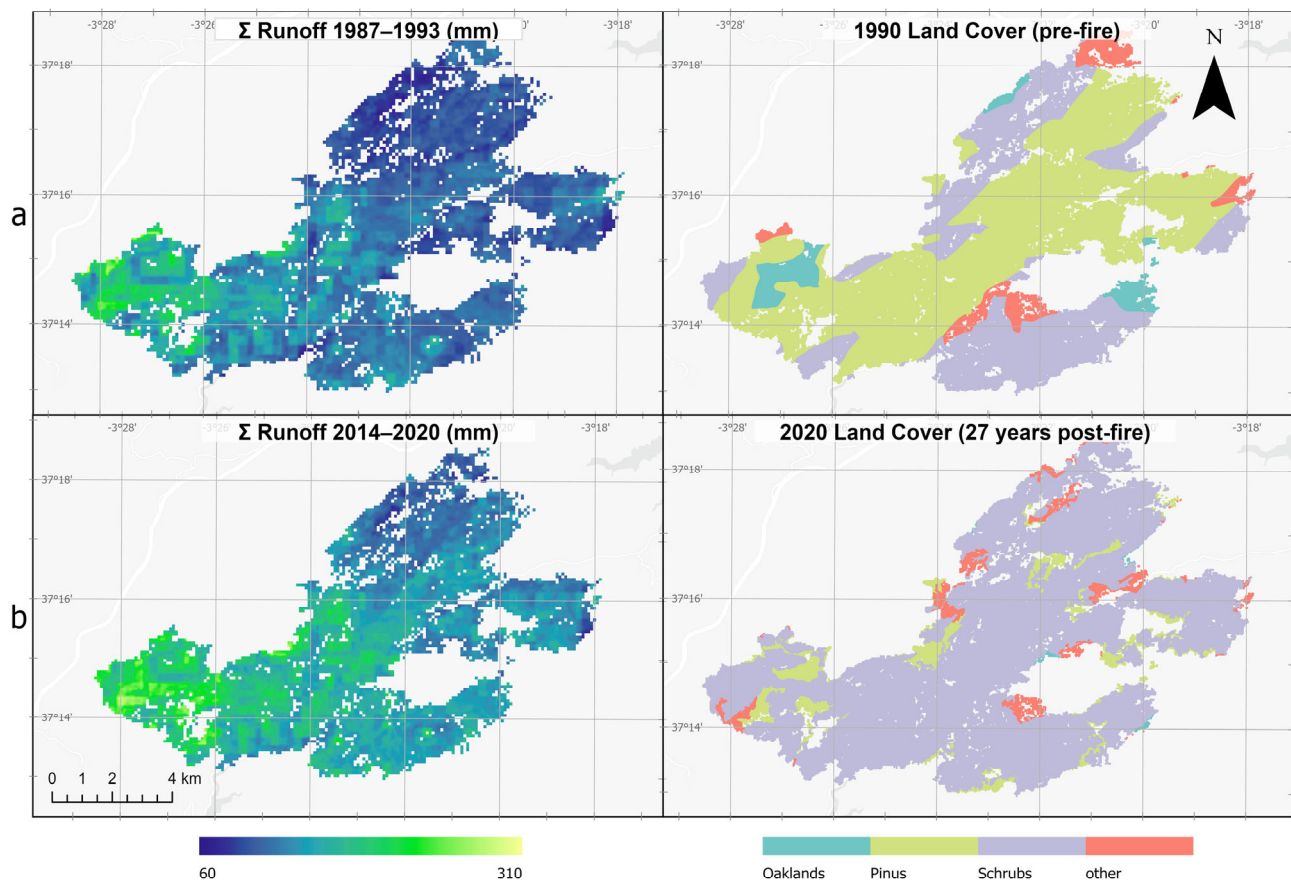


**Figure 4.** (a) Pre-fire vegetation conditions (Land Cover 1990) and runoff for the 1987–1993 period. *Pinus* forests dominated much of the watershed, associated with intermediate to lower runoff values (63.4–295.8 mm), whereas shrublands exhibited higher runoff levels. (b) Post-fire vegetation conditions (Land Cover 2020) and runoff for the 2014–2020 period. Twenty-five years after the fire, extensive areas were converted to shrublands, leading to increased spatial heterogeneity of runoff (67.4–302.5 mm).

### 3.3. Priority Post-Fire Restoration Index

The AHP was applied to assess the relative importance of selected environmental factors in reducing runoff and sediment yield under climate-change-related hazards (Table 1). For the reduction in runoff (“peak reduction” scenario), the most influential factors were runoff (0.30) and flow accumulation (0.19), followed by slope (0.15), distance to drainage network (0.11), LiDAR-derived structural complexity metrics (0.10), USLE erodibility factor K (0.09), and lithology (0.07). For sediment reduction, runoff (0.22), flow accumulation (0.18), USLE factor K (0.19), slope (0.17), distance to drainage network (0.14) were the dominant factors, while lithology (0.09), and LiDAR-derived metrics (0.03) had a lower influence. The CR values (0.002 and 0.015, respectively) indicated an acceptable level of consistency, below the 0.10 threshold (Tables S6 and S7, Supplementary Materials).

The spatial distribution of cumulative runoff between 2014 and 2020 highlights specific zones with a higher Priority Post-fire Restoration Index in the burned watershed that require urgent restoration measures (Figure 5, Table 2). Runoff values ranged from 67.4 to 302.5 mm, with the highest concentrations recorded in the northern and central sectors of the catchment, particularly in areas dominated by shrubland cover and fragmented *Pinus* stands (see Figures 1 and 4). These areas represented critical sources of runoff, where limited canopy cover and reduced soil infiltration promoted rapid hydrological responses during rainfall events. In contrast, areas occupied by oak forests consistently exhibited lower runoff values, showing higher hydrological stability and reduced susceptibility

to surface erosion. These findings suggest that oak-dominated patches act as stabilizing elements in the landscape, mitigating extreme runoff despite post-fire alterations in surrounding vegetation.

**Table 1.** Selected indicators for each of the components of risk and vulnerability for the three main climate-change hazards considered in this study (wildfires, drought, and pests) according to analytic hierarchy process (AHP). Consistency ratios (CR) of 0.10 and lower are considered tolerable.

Factor	Runoff	Sediments
Runoff (mm)	0.30	0.22
Flow accumulation (mm)	0.19	0.18
Distance to drainage network (m)	0.11	0.14
Slope (%)	0.15	0.17
Lithology	0.07	0.09
Erodibility factor K	0.09	0.19
LiDAR	0.10	0.03
CR	0.002	0.015

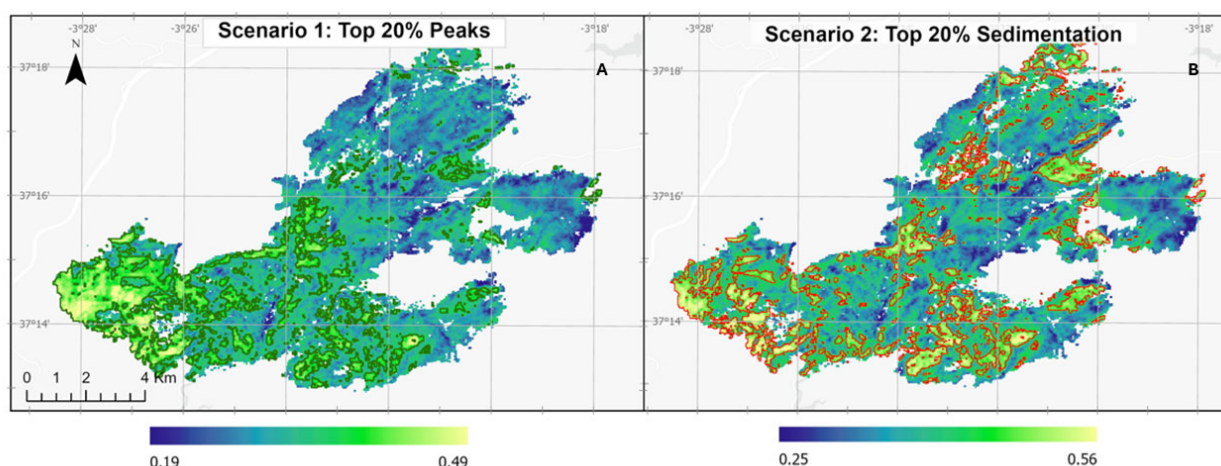


**Figure 5.** Potential Post-fire Restoration Index (PPRI) values: (A) peak reduction scenario index, (B) sediment reduction scenario in Sierra de Huetor (Granada, southern Spain). Areas with higher values of PPRI are highlighted.

**Table 2.** Surface area (ha) and percentage (%) distribution of hydrological and ecological variables across five categories (Very Low to Very High) in the study area. Variables include PPRI, sediment reduction scenario (SED), Priority Post-fire Restoration: peak reduction scenario (PEAKS).

Category	SED	PEAKS
High	<b>682.61 (10.06)</b>	<b>308.45 (4.55)</b>
Low	1376.48 (20.29)	1559.37 (22.98)
Middle	4647.88 (68.50)	4860.74 (71.64)
Very High	24.93 (0.37)	12.96 (0.19)
Very Low	52.92 (0.78)	43.29 (0.64)

Shrub-dominated areas in the north and central catchment, where high runoff values (>250 mm) coincide with steep slopes, increase the risk of soil erosion and downstream sediment delivery (Table 2). Degraded *Pinus* patches with incomplete canopy recov-

ery, where runoff values were intermediate to high, reflect insufficient interception and soil protection.

#### 4. Discussion

Post-fire hydrological processes and their evolution during vegetation recovery in Mediterranean watersheds are a key issue in post-fire forest restoration. The WiMMed model successfully reproduced the temporal dynamics of surface runoff and soil moisture in burned and unburned areas, demonstrating its sensitivity to vegetation structure and soil conditions derived from LiDAR and Landsat datasets.

##### 4.1. Hydrological Responses Under Post-Fire Conditions

The first objective of this study focused on representing post-fire fundamental hydrological processes such as infiltration, evapotranspiration, overland flow, and sediment transport through the WiMMed model. The results demonstrated the capacity of the model to reproduce rapid fluctuations in surface runoff (surface flow and runoff) alongside soil moisture dynamics in shallow and deeper layers. These dynamics were consistent with the expected responses of Mediterranean ecosystems to wildfire, where the removal of canopy cover and litter reduces interception and infiltration, leading to enhanced overland flow [32,33].

The sharp contrasts between soil moisture (HSol1 and HSol2) confirmed the importance of vertical differentiation in post-fire hydrological functioning. Shallow layers are directly exposed to precipitation inputs, responding with high soil moisture variability, while deeper horizons act as buffers with delayed responses. This increase in surface soil water content likely reflects the combined effects of vegetation removal, which reduced transpiration, and the formation of soil hydrophobic layers that limit infiltration to deeper horizons, leading to moisture accumulation in the upper soil profile. Similarly, previous study reported that wildfire reduces soil water holding capacity in the uppermost horizons [34], whereas deeper layers remain comparatively insulated from immediate disturbance. Therefore, the simulations obtained from WiMMed capture not only surface flow dynamics but also subsurface limitations on soil water redistribution, offering a useful approach that complements field measurements. The incorporation of statistical significance testing in the present study helps to distinguish robust temporal differences from natural interannual variability, but the magnitude of these differences should be interpreted within the context of parameter and input data uncertainty inherent to post-fire modeling.

Simulated surface runoff for burned and unburned areas in post-fire years reflected the immediate post-fire reduction in canopy interception and infiltration capacity due to vegetation loss and potential soil hydrophobicity, which together enhances overland flow generation. Local pulses of runoff are quickly transmitted to downstream outlets, reinforcing that post-fire landscapes are highly sensitive to rainfall extremes. This process is well documented in Mediterranean catchments, where short but intense rainfall events can generate disproportionate sediment and water fluxes [35,36]. The post-fire increase in runoff and surface soil moisture observed in our simulations is consistent with patterns documented in other Mediterranean basins, where canopy loss, reduced litter interception, and short-term declines in infiltration capacity have been shown to enhance hydrological response during the first decade after fire [37,38]. The subsequent attenuation of these effects over time aligns with studies demonstrating that the progressive recovery of shrub and pine cover increases evapotranspiration, restores surface roughness, and enhances soil structure, thereby reducing runoff generation and promoting the convergence toward pre-fire hydrological conditions. Thus, WiMMed provides an effective framework for quantifying short-term hydrological instability following fire. Accumulated lateral flow

(Qlat) for burned and unburned areas was related to surface and near-surface runoff due to vegetation loss, reduced interception, and potential development of hydrophobic layers that limit infiltration.

While vegetation recovery plays a dominant role in long-term hydrological stabilization, attributing all hydrological variation solely to vegetation would be reductive. Short-term post-fire hydrology is also shaped by fire-induced soil changes—such as temporary hydrophobicity, reduced infiltration, and surface sealing—as well as by spatial variability in burn severity. Likewise, differences in annual meteorological conditions contribute to hydrological variability. The WiMMed simulations incorporate these factors through severity-dependent adjustments to soil and surface parameters and by forcing the model with continuous multi-decadal climate data. Nonetheless, the interacting influences of vegetation, soils, and climate should be interpreted jointly when assessing modeled post-fire trajectories.

These results highlight the ability of the WiMMed model to reproduce the fundamental mechanisms of post-fire hydrological responses in Mediterranean watersheds. By integrating vertical soil moisture differentiation and lateral flow dynamics, the model captures the complex interplay between vegetation structure, soil properties, and hydrological connectivity that emerges after disturbance. The simulated responses reveal both the short-term destabilization of the hydrological system—driven by canopy loss and surface sealing—and the gradual re-establishment of equilibrium as vegetation and soil functions recover.

#### *4.2. Integration of Remote Sensing and Field Data for Improved Simulations*

The integration of remote sensing and field data was fundamental to the enhancement in the performance and interpretability of WiMMed simulations in Mediterranean watersheds after fires. Remote sensing datasets provided a synoptic and temporally consistent characterization of vegetation and surface conditions that complemented the model-based measurements. LiDAR data offered high-resolution three-dimensional information on canopy height, structural complexity, and vegetation density, enabling a detailed representation of interception capacity and aerodynamic roughness in the model [39]. These variables are critical for the simulation of rainfall partitioning, evapotranspiration, and infiltration processes that are strongly modified after fire disturbance. By quantifying canopy loss and subsequent regrowth, LiDAR-derived metrics allowed the model to incorporate structural vegetation recovery directly into hydrological parameterization, thereby improving the temporal realism of simulated post-fire responses.

Complementing this structural information, Landsat imagery provided multi-decadal temporal coverage that captured the spatial variability of vegetation regrowth [9]. Vegetation indices (e.g., NDVI) were employed to monitor the gradual recovery of photosynthetic activity and surface greenness, serving as proxies for changes in interception, transpiration, and soil exposure. This temporal integration facilitated the representation of hydrological trends during the vegetation recovery period, linking remote-sensing-derived vegetation dynamics to hydrological parameters within the WiMMed framework. Therefore, the combined use of LiDAR and Landsat data cover the scale gap between localized field observations and distributed hydrological model simulations, ensuring that the model reflected both fine-scale vegetation structure and broader landscape patterns of vegetation recovery.

The integration of multi-source data within the WiMMed modeling framework significantly enhanced the capacity to represent the coupled ecohydrological processes driving post-fire recovery. The synergy between remote sensing and process-based modeling provided a comprehensive understanding of watershed-scale hydrological responses and

vegetation resilience mechanisms. This integrative approach not only strengthens confidence in model output but also supports the development of spatially explicit restoration and management strategies. By coupling detailed vegetation recovery monitoring with hydrological simulations, this study demonstrates how remote sensing can be effectively leveraged to improve predictive modeling and inform adaptive management in fire-prone Mediterranean landscapes.

#### 4.3. Identification of Priority Areas for Restoration and Management

The third objective of this study was to identify critical source areas of runoff and erosion to inform targeted restoration interventions. The development of the PPRI through the AHP provided a structured framework to identify critical areas for restoration based on their hydrological vulnerability and sediment risk under post-fire conditions. The weighting scheme revealed that runoff and flow accumulation were the most influential factors in reducing peak discharge, while slope and distance to drainage dominated sediment reduction priorities. The validity of the PPRI is supported by several factors. First, the AHP weighting procedure achieved acceptable consistency ratios ( $CR < 0.10$ ), and expert judgment distributions (Tables S6 and S7, Supplementary Materials) supporting their reliability for spatial prioritization. Second, the spatial pattern of high-PPRI areas aligns with zones known to generate high runoff and sediment loads after the 1993 fire and in comparable Mediterranean basins [17]. Third, sensitivity tests with  $\pm 20\%$  variation in weights produced stable priority-area patterns, demonstrating robustness to subjective uncertainty. Together, these elements support the reliability of the PPRI as a decision-support tool for identifying critical restoration areas.

The proposed Priority Post-Fire Restoration Index (PPRI) for assigning areas of restoration priority to reduce runoff peaks and/or volumes of sediment transport allowed us to highlight that shrub-dominated sectors in the northern and central parts of the watershed generate the highest cumulative runoff (often exceeding 250 mm). These areas represent hydrological “hotspots,” where the combination of limited canopy cover, shallow rooting systems, and steep slopes increases the risk of soil erosion and downstream sediment delivery [40]. Conversely, oak woodlands consistently showed lower runoff values, emphasizing their stabilizing influence on the landscape. The PPRI has strong management implications: promoting oak regeneration in burned Mediterranean landscapes may be more effective in the long term than relying solely on pine reforestation, which remains vulnerable to recurrent fires. With their resprouting ability and deeper rooting systems, oaks can enhance infiltration and water retention while reducing erosion [41]. These results are consistent with the understanding that, in Mediterranean landscapes, steep terrain and drainage proximity are key drivers of both surface runoff concentration and sediment transport [42].

The identification of priority zones through the PPRI provides a spatial framework for implementing targeted restoration measures, but assessing their likely effectiveness is essential for management planning. In Mediterranean post-fire landscapes, interventions such as reforestation with deep-rooted native species (e.g., *Quercus ilex*) have been shown to enhance infiltration, increase soil cohesion, and promote long-term reductions in runoff and sediment yield compared with pine-based reforestation strategies [42]. The high-PPRI areas identified in this study, characterized by steep slopes, degraded shrublands, and high hydrological connectivity, were located where these vegetation-based interventions are expected to produce the largest hydrological benefits by increasing surface roughness, restoring evapotranspiration, and stabilizing soils. In addition, structural measures such as contour-felled logs, check dams, and sediment barriers have historically proven effective in Mediterranean watersheds by interrupting overland flow paths, reducing peak discharges,

and trapping sediments during early post-fire years when hydrological responses are most extreme [43]. Implementing such measures within the PPRI-defined corridors of concentrated runoff would likely mitigate downstream sediment delivery and reduce the magnitude of post-fire flash floods. Historical restoration efforts in the region, including early interventions following the 1993 Sierra de Huétor fire, demonstrated that even partial coverage of erosion control structures contributed to improved soil moisture retention and reduced sediment mobilization, despite limited long-term maintenance.

Additionally, the identification of connectivity corridors between high-runoff zones further underscores the role of landscape structure in shaping hydrological risk. Concentrated flows along these pathways increase the likelihood of sediment delivery into downstream reservoirs, threatening water quality and storage capacity. Prioritizing interventions in such corridors—through soil stabilization measures, check dams, or vegetative buffer strips—can disrupt runoff connectivity and reduce the cumulative impacts of post-fire hydrological extremes [44]. The use of WiMMed to integrate hydrological simulations with spatial land cover information provides a valuable decision-support framework for restoration planning. By identifying critical restoration areas based on PPRI, managers can allocate resources more efficiently, targeting interventions where they will deliver the greatest reduction in erosion and runoff risks. This approach aligns with emerging strategies in adaptive watershed management, which emphasize spatial prioritization and ecosystem-based restoration.

#### 4.4. Broader Implications and Limitations

Spatial patterns of cumulative runoff from 2014 to 2020 revealed pronounced hydrological contrasts within the burned watershed. The highest runoff values were concentrated in the northern and central sectors, primarily in shrub-dominated and fragmented *Pinus* stands, where incomplete canopy recovery and limited litter cover continue to enhance surface flow and erosion susceptibility. In contrast, oak woodlands consistently exhibited lower runoff and sediment potential, reflecting their greater soil stability, deeper rooting systems, and higher infiltration capacity. These patterns confirm the critical role of vegetation type and structural complexity in modulating post-fire hydrological responses and reinforce the importance of mixed stands of native species in promoting watershed resilience [2].

The PPRI maps derived from both “peak reduction” and “sediment reduction” scenarios highlight spatial heterogeneity in restoration needs. Under the peak reduction scenario, priority zones were associated with areas exhibiting concentrated runoff pathways and moderate-to-steep slopes, which function as hydrological connectors transmitting flow toward downstream reservoirs [45]. The sediment reduction scenario emphasized zones near drainage networks and steep slopes where soil detachment and transport are most likely. The convergence of high runoff and sediment indices in specific sub-catchments suggests that these locations function as “hydrological hotspots,” where restoration interventions would yield the greatest cumulative benefit in terms of reductions in flood and erosion risks. Over 65% of the study area falls within the “middle” restoration priority category, indicating a landscape in partial recovery, yet still vulnerable to extreme rainfall events. A smaller proportion (approximately 10%) corresponds to high-priority areas requiring immediate restoration interventions, often characterized by degraded soils, sparse vegetation, and high topographic connectivity. These findings provide a quantitative basis for optimizing restoration strategies, allowing managers to allocate limited resources to the most sensitive zones.

The integration of WiMMed hydrological outputs with LiDAR- and Landsat-derived indicators within a Priority Post-Fire Restoration Index (PPRI) framework represents a key

advancement in post-fire landscape management. This combined approach allows for a multi-criteria evaluation that merges process-based understanding with spatially explicit data, capturing both the physical and biological dimensions of watershed recovery. By linking hydrological modeling to remote sensing-derived vegetation and terrain metrics, the PPRI effectively translates complex ecohydrological processes into practical spatial information. Such integration supports the design of adaptive, data-driven restoration strategies such as reforestation with deep-rooted native species, constructions of check dams, and establishment of vegetated buffer strips to interrupt runoff connectivity and stabilize sediments.

While the analysis presented here was based on a single, well-documented wildfire, the methodological approach has broader applicability. The use of distributed, physically based hydrological modeling (WiMMed) combined with LiDAR–Landsat vegetation metrics enables simulation of post-fire hydrological dynamics across a wide range of fire regimes and landscape contexts [9,15]. Because these tools are scalable, the framework can be applied to more recent fires, events with different burn severities, or regions with contrasting geology and vegetation. Likewise, the PPRI structure allows weighting factors to be recalibrated to local management objectives, making the methodology adaptable to other Mediterranean watersheds and to fire-prone ecosystems worldwide.

Several sources of uncertainty should be acknowledged when interpreting the PPRI results. First, the hydrological simulations depend on the parameterization of WiMMed, particularly  $K_s$ ,  $S_{max}$ , Manning's  $n$ , and  $ET/ET_0$ , which, even after calibration, may propagate uncertainty into modeled runoff, soil moisture, and lateral flow responses. Second, input datasets also contribute uncertainty: the coarse spatial resolution of ERA5-Land climatic forcing may underrepresent fine-scale precipitation variability, and LiDAR- or Landsat-derived vegetation metrics, despite rigorous preprocessing, remain subject to sensor limitations and model inversion errors. Third, the AHP-based weighting scheme used to construct the PPRI relies on expert judgment, which can introduce subjective bias despite the acceptable consistency ratios obtained. Although sensitivity tests showed that the spatial pattern of priority areas was largely robust to moderate changes in weighting factors, some variability in PPRI classification should still be expected. Future studies could further reduce these uncertainties by incorporating ensemble-based parameter estimation, higher-resolution climatic data, and alternative multi-criteria weighting frameworks.

## 5. Conclusions

The WiMMed model was able to represent post-fire hydrological processes, capturing both short-term runoff pulses and vertical differentiation of soil moisture. Integrating remote sensing land cover maps and hydrological models improves calibration, enabling reliable simulations of key hydrological variables across pre- and post-fire scenarios. Identifying critical runoff source areas allows for targeted restoration actions. In this study, oak forests emerged as key stabilizing vegetation in long-term recovery. This work contributed to assessing and managing the hydrological impacts of wildfire in Mediterranean environments. The results underscore the importance of considering both ecological succession and hydrological connectivity when designing post-fire restoration strategies, thereby supporting adaptive and risk-based restoration management approaches in fire-prone regions. The PPRI demonstrates the utility of combining process-based modeling and remote sensing to identify and prioritize restoration zones in Mediterranean watersheds affected by wildfires. The approach not only highlights areas of persistent hydrological instability but also provides a replicable methodology that can be applied to other fire-prone regions under climate change scenarios.

**Supplementary Materials:** The following supporting information can be downloaded at: <https://www.mdpi.com/article/10.3390/rs18010026/s1>, Table S1: Metrics of airborne laser scanning (ALS) used for individual tree characterization; Table S2: Performance metrics of Lidar-Landsat models. Metrics include Coefficient of Determination ( $R^2$ ), Root Mean Square Error (RMSE), Percent RMSE (%RMSE), Bias, and Mean Absolute Error (MAE); Table S3: Input data used in hydrological simulations; Table S4: Effects of fire severity on hydrological functioning, soil and surface parameters; Table S5: Output data used in hydrological simulations; Table S6: Pairwise comparison matrix (mean values) for the peak-reduction scenario; Table S7: Pairwise comparison matrix (mean values) for the sediment-reduction scenario; Figure S1: Flowchart illustrates the WiMMed hydrological modeling workflow, including data inputs (DEM, soil map, climate data) and model outputs (Exp, HSol1, HSol2, Qlat). References [46–48] are cited in the Supplementary Materials.

**Author Contributions:** Conceptualization, R.M.N.C. and E.A.V.P.; methodology, R.M.N.C. and E.A.V.P.; software, E.A.V.P. and R.M.N.C.; validation, E.A.V.P. and R.M.N.C.; formal analysis, E.A.V.P. and R.M.N.C.; investigation, R.M.N.C. and E.A.V.P.; resources, R.M.N.C.; data curation, E.A.V.P.; writing—original draft preparation, R.M.N.C. and E.A.V.P.; writing—review and editing, R.M.N.C. and E.A.V.P.; visualization, E.A.V.P.; supervision, R.M.N.C.; project administration, R.M.N.C.; funding acquisition, R.M.N.C. All authors have read and agreed to the published version of the manuscript.

**Funding:** This research was funded by which has the support of the Biodiversity Foundation of the Ministry for the Ecological Transition and the Demographic Challenge (MITECO) of the Government of Spain, within the framework of the Recovery, Transformation and Resilience Plan (PRTR), funded by the European Union–NextGenerationEU.

**Data Availability Statement:** Data used and outputs obtained are available through request.

**Acknowledgments:** We acknowledge the institutional support of the Consejería de Sostenibilidad y Medio Ambiente. (Junta de Andalucía) for providing data support. R.M.N.C. acknowledge the support of REFLORESTA, (“Innovación tecnológica, social y en gobernanza para mejorar la prevención y acelerar la recuperación de los ecosistemas y paisajes afectados por incendios”), Programa Interreg España-Portugal (POCTEP) 2021–2027. We thank Jorgelina Brasca for revisions of the written English in different versions of this manuscript.

**Conflicts of Interest:** The authors declare no conflicts of interest.

## Abbreviations

The following abbreviations are used in this manuscript:

WiMMed	Watershed Integrated Management in Mediterranean Environments
LiDAR	Light Detection and Ranging
AHP	Analytic Hierarchy Process
PPRI	Priority Post-Fire Restoration Index

## References

1. Mansoor, S.; Farooq, I.; Kachroo, M.; Mahmoud, A.; Fawzy, M.; Popescu, S.; Ahmad, P. Elevation in wildfire frequencies with respect to the climate change. *J. Environ. Manag.* **2022**, *301*, 113769. [[CrossRef](#)]
2. Moazeni, S.; Cerdà, A. The impacts of forest fires on watershed hydrological response. A review. *Trees For. People* **2024**, *18*, 100707. [[CrossRef](#)]
3. Moreira, F.; Leal, M.; Bergonse, R.; Canadas, M.J.; Novais, A.; Oliveira, S.; Santos, J.L. Recent trends in fire regimes and associated territorial features in a fire-prone Mediterranean region. *Fire* **2023**, *6*, 60. [[CrossRef](#)]
4. González-Pelayo, O.; Prats, S.A.; van den Elsen, E.; Malvar, M.C.; Ritsema, C.; Bautista, S.; Keizer, J.J. The effects of wildfire frequency on post-fire soil surface water dynamics. *Eur. J. For. Res.* **2024**, *143*, 493–508. [[CrossRef](#)]
5. Li, Q.; Ahn, S.; Kim, T.; Im, S. Post-fire impacts of vegetation burning on soil properties and water repellency in a pine forest, South Korea. *Forests* **2021**, *12*, 708. [[CrossRef](#)]
6. Smith, H.; Sheridan, G.; Lane, P.; Nyman, P.; Haydon, S. Wildfire effects on water quality in forest catchments: A review with implications for water supply. *J. Hydrol.* **2011**, *396*, 170–192. [[CrossRef](#)]

7. Riley, K.; Bendick, R.; Hyde, K.; Gabet, E. Frequency–magnitude distribution of debris flows compiled from global data, and comparison with post-fire debris flows in the western US. *Geomorphology* **2013**, *191*, 118–128. [[CrossRef](#)]
8. Viana-Soto, A.; García, M.; Aguado, I.; Salas, J. Assessing post-fire forest structure recovery by combining LiDAR data and Landsat time series in Mediterranean pine forests. *Int. J. Appl. Earth Obs. Geoinf* **2022**, *108*, 102754. [[CrossRef](#)]
9. Velasco-Pereira, E.; Navarro-Cerrillo, R.M. Post-fire regeneration dynamics of heterogeneous Mediterranean ecosystems using Landsat and ALS data. *Sci. Total Environ.* **2025**, *1001*, 180435. [[CrossRef](#)]
10. McCarley, T.R.; Kolden, C.A.; Vaillant, N.; Hudak, A.; Smith, A.; Wing, B.; Kreitler, J. Multi-temporal LiDAR and Landsat quantification of fire-induced changes to forest structure. *Remote Sens. Environ.* **2017**, *191*, 419–432. [[CrossRef](#)]
11. Niemeyer, R.; Bladon, K.; Woodsmith, R.D. Long-term hydrologic recovery after wildfire and post-fire forest management in the interior Pacific Northwest. *Hydrol. Process.* **2020**, *34*, 1182–1197. [[CrossRef](#)]
12. Boyer, E.W.; Wagenbrenner, J.W.; Zhang, L. Wildfire and hydrological processes. *Hydrol. Process.* **2022**, *36*, e14640. [[CrossRef](#)]
13. Herrero, J.; Millares Valenzuela, A.; Moreno Llorca, R. Outputs of the WiMMed Hydrological Model for Sierra Nevada (Spain). 2023. Available online: <https://produccioncientifica.ugr.es/documentos/668fc432b9e7c03b01bd615b?lang=en> (accessed on 3 February 2025).
14. Egüen, M.; Aguilar, C.; Herrero, J.; Millares, A.; Polo, M.J. On the influence of cell size in physically based distributed hydrological modelling to assess extreme values in water resource planning. *Nat. Hazards Earth Syst. Sci.* **2012**, *12*, 1573–1582. [[CrossRef](#)]
15. Ebel, B.A.; Shephard, Z.M.; Walvoord, M.A.; Murphy, S.F.; Partridge, T.F.; Perkins, K.S. Modeling post-wildfire hydrologic response: Review and future directions for applications of physically based distributed simulation. *Earth's Future* **2023**, *11*, e2022EF003038. [[CrossRef](#)]
16. Key, C.H.; Benson, N.C. Landscape assessment (LA). In *FIREMON: Fire Effects Monitoring and Inventory System*; Lutes, D.C., Keane, R.E., Caratti, J.F., Key, C.H., Benson, N.C., Sutherland, S., Gangi, L.J., Eds.; US Department of Agriculture, Forest Service, Rocky Mountain Research Station: Fort Collins, CO, USA, 2006; Volume 164, p. LA-1-55.
17. Hernández-Clemente, R.; Navarro-Cerrillo, R.M.; Gitas, I.Z. Monitoring post-fire regeneration in Mediterranean ecosystems by employing multitemporal satellite imagery. *Int. J. Wildland Fire* **2009**, *18*, 648–658. [[CrossRef](#)]
18. de Andalucía, J. Sistema de Información Sobre el Patrimonio Natural de Andalucía. 2021. Available online: [https://www.juntadeandalucia.es/medioambiente/portal/landing-page-%C3%ADndice/-/asset\\_publisher/zX2ouZa4r1Rf/content/sistema-de-informaci-c3-b3n-sobre-el-patrimonio-natural-de-andaluc-c3-ada-sipna-/20151](https://www.juntadeandalucia.es/medioambiente/portal/landing-page-%C3%ADndice/-/asset_publisher/zX2ouZa4r1Rf/content/sistema-de-informaci-c3-b3n-sobre-el-patrimonio-natural-de-andaluc-c3-ada-sipna-/20151) (accessed on 11 January 2025).
19. PNOA. Available online: <https://centrodedescargas.cnig.es/CentroDescargas/home> (accessed on 11 January 2025).
20. Isenburg, M. *LAStools*; Rapidlasso GmbH: Gilching, Germany, 2017.
21. Roussel, J.; Auty, D.; Coops, N.; Tompalski, P.; Goodbody, T.; Meador, A.; Achim, A. lidR: An R package for analysis of Airborne Laser Scanning (ALS) data. *Remote Sens. Environ.* **2020**, *251*, 112061. [[CrossRef](#)]
22. Schowengerdt, R.A. *Techniques for Image Processing and Classifications in Remote Sensing*; Academic Press: New York, NY, USA, 2012.
23. Soenen, S.A.; Peddle, D.R.; Coburn, C.A. SCS+ C: A modified sun-canopy-sensor topographic correction in forested terrain. *IEEE Trans. Geosci. Remote Sens.* **2005**, *43*, 2148–2159. [[CrossRef](#)]
24. Beven, K.J.; Kirkby, M.J. A physically based, variable contributing area model of basin hydrology. *Hydrol. Sci. J.* **1979**, *24*, 43–69. [[CrossRef](#)]
25. Van, L.N.; Lee, G. Investigating the Relationship Between Topographic Variables and Wildfire Burn Severity. *Geographies* **2025**, *5*, 47. [[CrossRef](#)]
26. REDIAM. Available online: [https://portalrediam.cica.es/caracterizacion\\_vegetacion/sipna.html](https://portalrediam.cica.es/caracterizacion_vegetacion/sipna.html) (accessed on 11 January 2025).
27. Moreno, I.; Millares, A.; Herrero, J.; Losada, M.A.; Aguilar, C.; Polo, M.J. WiM-Med, un modelo de gestión hidrológica a escala de cuenca. IV Congreso Andaluz de Desarrollo Sostenible/VIII Congreso Andaluz de Ciencias Ambientales. (Calibrated for the Guadalfeo basin, Andalusia). 2009. Available online: [https://digibug.ugr.es/bitstream/handle/10481/62222/Moreno\\_2009\\_Ambientalia.pdf?sequence=1&isAllowed=y](https://digibug.ugr.es/bitstream/handle/10481/62222/Moreno_2009_Ambientalia.pdf?sequence=1&isAllowed=y) (accessed on 23 February 2025).
28. R Core Team. *R: A Language and Environment for Statistical Computing*; R Foundation for Statistical Computing: Vienna, Austria, 2024; Available online: <https://www.R-project.org/> (accessed on 11 January 2025).
29. Inbar, A.; Lado, M.; Sternberg, M.; Tenau, H.; Ben-Hur, M. Forest fire effects on soil chemical and physicochemical properties, infiltration, runoff, and erosion in a semiarid Mediterranean region. *Geoderma* **2014**, *221*, 131–138. [[CrossRef](#)]
30. Saaty, T.L. Decision making with the analytic hierarchy process. *Int. J. Serv. Sci.* **2008**, *1*, 83–98. [[CrossRef](#)]
31. He, J.; Li, Y.; Zhou, W.; Qian, M.; Zha, E.; Shi, X. A Multi-Objective Framework for Regional Ecological Planning: Restoration Prioritization Analysis. *Land Degrad. Dev.* **2025**, *36*, 3670–3684. [[CrossRef](#)]
32. Roche, P.K.; Campagne, C.S.; Ganteaume, A. Post-fire Recovery Dynamics and Resilience of Ecosystem Services Capacity in Mediterranean-Type Ecosystems. *Ecosystems* **2024**, *27*, 833–847. [[CrossRef](#)]
33. Ermitão, T.; Gouveia, C.M.; Bastos, A.; Russo, A.C. Recovery following recurrent fires across Mediterranean ecosystems. *Glob. Change Biol.* **2024**, *30*, e70013. [[CrossRef](#)] [[PubMed](#)]

34. Pereira, P.; Cerdà, A.; Úbeda, X.; Mataix-Solera, J.; Rein, G. (Eds.); *Fire Effects on Soil Properties*; CSIRO Publishing: Canberra, Australia, 2019.
35. Mayor, A.G.; Bautista, S.; Llovet, J.; Bellot, J. Post-fire hydrological and erosional responses of a Mediterranean landscape: Seven years of catchment-scale dynamics. *Catena* **2007**, *71*, 68–75. [[CrossRef](#)]
36. Rosso, R.; Rulli, M.C.; Bocchiola, D. Transient catchment hydrology after wildfires in a Mediterranean basin: Runoff, sediment and woody debris. *Hydrol. Earth Syst. Sci.* **2007**, *11*, 125–140. [[CrossRef](#)]
37. Shakesby, R.A.; Doerr, S.H. Wildfire as a hydrological and geomorphological agent. *Earth-Sci. Rev.* **2006**, *74*, 269–307. [[CrossRef](#)]
38. Cerdà, A.; Doerr, S.H. The effect of ash and needle cover on surface runoff and erosion in the immediate post-fire period. *Catena* **2008**, *74*, 256–263. [[CrossRef](#)]
39. Goodwin, N.R.; Coops, N.C.; Culvenor, D.S. Development of a simulation model to predict LiDAR interception in forested environments. *Remote Sens. Environ.* **2007**, *111*, 481–492. [[CrossRef](#)]
40. Liu, Y.F.; Dunkerley, D.; Lopez-Vicente, M.; Shi, Z.H.; Wu, G.L. Trade-off between surface runoff and soil erosion during the implementation of ecological restoration programs in semiarid regions: A meta-analysis. *Sci. Total Environ.* **2020**, *712*, 136477. [[CrossRef](#)]
41. Lewis, D.; Singer, M.J.; Dahlgren, R.A.; Tate, K.W. Hydrology in a California oak woodland watershed: A 17-year study. *J. Hydrol.* **2000**, *240*, 106–117. [[CrossRef](#)]
42. Fortesa, J.; Latron, J.; García-Comendador, J.; Company, J.; Estrany, J. Runoff and soil moisture as driving factors in suspended sediment transport of a small mid-mountain Mediterranean catchment. *Geomorphology* **2020**, *368*, 107349. [[CrossRef](#)]
43. Papaioannou, G.; Alamanos, A.; Maris, F. Evaluating post-fire erosion and flood protection techniques: A narrative review of applications. *GeoHazards* **2023**, *4*, 380–405. [[CrossRef](#)]
44. Lucas-Borja, M.E. Efficiency of postfire hillslope management strategies: Gaps of knowledge. *Curr. Opin. Environ. Sci. Health* **2021**, *21*, 100247. [[CrossRef](#)]
45. Liu, G.; Shao, Q.; Fan, J.; Huang, H.; Liu, J.; He, J. Assessment of restoration degree and restoration potential of key ecosystem-regulating services in the three-river headwaters region based on vegetation coverage. *Remote Sens.* **2023**, *15*, 523. [[CrossRef](#)]
46. Herrero, J.; Millares, A.; Aguilar, C.; Egüen, M.; Losada, M.A. Coupling spatial and time scales in the hydrological modelling of mediterranean regions: WiMMed. In *CUNY Academic Works, Proceedings of the 11th International Conference on Hydroinformatics HIC 2014, New York, NY, 17–21 August 2014*; City University of New York (CUNY): New York, NY, USA, 2014; p. 8.
47. ITGE-Junta de Andalucía. *Atlas Hidrogeológico de Andalucía*; IGME: Madrid, Spain, 1998; 216p, ISBN 84-7840-351-5. Available online: [https://web.igme.es/actividadesigme/lineas/HidroyCA/publica/libros1\\_HR/libro110/lib110.htm](https://web.igme.es/actividadesigme/lineas/HidroyCA/publica/libros1_HR/libro110/lib110.htm) (accessed on 11 January 2025).
48. Herrero, J.; Aguilar, C.; Millares, A.; Polo, M.J. *WiMMed MANUAL DE USUARIO V 2.0*; Grupo de Dinámica Fluvial e Hidrología, Universidad de Córdoba: Córdoba, Spain; Grupo de Dinámica de Flujos Ambientales Centro Andaluz de Medio Ambiente (CEAMA), Universidad de Granada: Granada, Spain, 2013.

**Disclaimer/Publisher’s Note:** The statements, opinions and data contained in all publications are solely those of the individual author(s) and contributor(s) and not of MDPI and/or the editor(s). MDPI and/or the editor(s) disclaim responsibility for any injury to people or property resulting from any ideas, methods, instructions or products referred to in the content.